



 Cite this: *RSC Adv.*, 2018, 8, 5740

Synthesis of Cu₂O–CuFe₂O₄ microparticles from Fenton sludge and its application in the Fenton process: the key role of Cu₂O in the catalytic degradation of phenol

 Muhammad Faheem, Xinbai Jiang,* Lianjun Wang and Jinyou Shen *

This paper presents the key role of Cu₂O in Fenton catalysis using Cu₂O–CuFe₂O₄ magnetic microparticles, which were prepared using Fenton sludge as an iron source. The catalytic activity of the as-prepared Cu₂O–CuFe₂O₄ and CuFe₂O₄ microparticles was evaluated in a heterogeneous Fenton system for the degradation of recalcitrant phenol. The Cu₂O–CuFe₂O₄ microparticles demonstrated relatively superior catalytic performance as compared to CuFe₂O₄ microparticles when used as a Fenton catalyst. The relatively higher catalytic activity of Cu₂O–CuFe₂O₄ for phenol degradation during the Fenton process could be attributed to the availability of both monovalent [Cu(I)] and divalent [Cu(II)] as well as Fe(II)/Fe(III) redox pairs, which could react quickly with H₂O₂ to generate hydroxyl radicals (HO[•]). An electron bridge was formed between Cu(I) and Fe(III), which accelerates the formation of Fe(II) species in order to boost the reaction rate. Highly reactive and excessively available Cu(I) species for as prepared Cu₂O–CuFe₂O₄ microparticles could be considered to be rather crucial for the generation of highly reactive HO[•] radical species. In addition, the as-prepared Cu₂O–CuFe₂O₄ magnetic microparticles exhibited sound stability and reusability.

 Received 23rd December 2017
 Accepted 30th January 2018

DOI: 10.1039/c7ra13608k

rsc.li/rsc-advances

1. Introduction

Fenton oxidation technology, which is well known as advanced oxidation processes (AOPs), has been extensively used to remove various recalcitrant or non-biodegradable organic pollutants from industrial wastewater.^{1,2} During Fenton process, a powerful oxidant, hydroxyl radicals (HO[•]) can be generated efficiently at near-ambient temperature and pressure by the reaction between Fe²⁺ and H₂O₂.³ The distinct properties of generated hydroxyl radicals (HO[•]) such as strong oxidation potential ($E^0 = 2.8$ V) and non-selective reactivity are considered to be responsible for the effectiveness of AOPs in the field of organic pollutant elimination. These generated radicals can react with a variety of organic pollutants, causing efficient degradation, even complete mineralization.^{4,5} However, in spite of the simplicity of Fenton process, bulk quantity of iron sludge generated during neutralization after Fenton oxidation restricts its implementation on large scale due to the increasing cost for Fenton sludge treatment and disposal to avoid environment deterioration.⁶

Two approaches have been implemented to reduce the Fenton sludge generation yield, *i.e.*, development of

heterogeneous iron bearing catalyst and reuse of Fenton sludge as iron source. Various heterogeneous catalysts have been synthesized, such as nano scale zero-valent iron,⁷ iron-containing clays,⁸ natural minerals,⁹ iron exchanged zeolite,¹⁰ and some solid support immobilized by iron.^{11,12} Immobilization of iron within the interlayer of heterogeneous catalysts results in relatively high oxidation performance. Moreover, heterogeneous catalysts have been proven to be superior to classical homogeneous catalysts *i.e.*, Fe²⁺, because they are easily separated from wastewater treatment system through applied magnetic field or simple sedimentation. Yoo *et al.*, suggested the recycling of iron incorporated sludge produced in Fenton oxidation system as coagulant during coagulation process.¹³ Through the recycling of Fenton sludge as coagulant, coagulant dosage could be lowered by 50% and sludge disposal could be decreased by 50%. Recycling of iron incorporated sludge also follows the 3R's rules regarding integrated solid waste management, *i.e.*, reduce, reuse and recycle. Iron sludge-graphene composite with low amount of graphene were synthesized as a heterogeneous Fenton catalyst by using iron sludge as the iron precursor. The as-prepared catalyst showed wide pH operating range, excellent stability, and was efficient for the degradation of acid red G and metronidazole.¹⁴ Zhang *et al.* synthesized magnetic biochar catalyst by using ferric sludge and biological sludge *via* hydrothermal process. This catalyst showed excellent characteristics to promote a heterogeneous Fenton reaction in methylene blue treatment.¹⁵ These

Jiangsu Key Laboratory of Chemical Pollution Control and Resources Reuse, School of Environmental and Biological Engineering, Nanjing University of Science and Technology, Nanjing 210094, Jiangsu Province, China. E-mail: xinbai_jiang@njust.edu.cn; shenjinyou@mail.njust.edu.cn; Fax: +86 25 84315941; +86 25 84303965; Tel: +86 25 84315941; +86 25 84303965



methods hold promise for ferric sludge waste reclamation and heterogeneous Fenton catalyst fabrication.

In addition to the recycling of iron incorporated sludge, the use of low cost heterogeneous catalyst in Fenton treatment could be another alternative for the reduction of hazardous ferric sludge. Recently, different approaches have been investigated to boost up the performance of synthesized heterogeneous Fenton catalyst, *e.g.*, to reduce the catalyst size up to nano-scale in order to increase surface energy and available active sites, to embed appropriate transition metal (Cu, Ni, V, Ti, Cr, Zn, Mn and Co, *etc.*) into the skeleton of Fe₃O₄ to improve the catalyst performance.¹⁶ The improvement of heterogeneous catalyst performance as a result of transition metals embedment into Fe₃O₄ structure could be attributed to the synergetic effect between newly inserted transition metal and Fe³⁺. This synergetic effect could be described by formation of galvanic cell between embedded transition metal and Fe³⁺. The improvement in catalyst activity could be ascribed to formation of redox pairs Fe³⁺/Fe²⁺ due to rapid electron flow as a result of transition metal insertion into Fe₃O₄ structure. A newly developed material can be implemented in different fields if it holds the properties of higher reactivity, sound stability and easy separation from reaction medium.

Mixed iron oxides or ferrites have drawn much more attention of scientist and researcher due to their ability to apply in different fields such as microwave devices,¹⁷ catalysis or catalyst,¹⁸ magnetic fluids¹⁹ and gas sensors.²⁰ Recently, various ferrites such as ZnFe₂O₄ (ref. 21) and CuFe₂O₄,²² and iron-copper bimetallic nanoparticles embedded within ordered mesoporous carbon composite,²³ have been utilized as the catalyst for heterogeneous Fenton like process to remove organic contaminants from wastewater. In our previous study, NiFe₂O₄ were synthesized through co-precipitation method followed by sintering at 800 °C.²⁴ In the Fenton system using NiFe₂O₄ as heterogeneous catalyst, phenol removal efficiency as high as 95 ± 3.4% could be achieved, indicating excellent catalytic performance of NiFe₂O₄ in the heterogeneous Fenton process. Roonasi and Nezhad carried out a comparative study to investigate the performance of synthetic M-ferrite nanoparticles (M = Cu, Zn, Fe or Mn) in heterogeneous catalysis. Among these ferrite nanoparticles, CuFe₂O₄ was found to be the best catalyst for phenol removal, as 78% of 100 mg L⁻¹ phenol could be efficiently removed within 175 min.²⁵ In addition, the effectiveness of Cu(I) species as compare to Cu(II) species for the activation of H₂O₂ in order to generate HO· radicals for the degradation of bisphenol has been confirmed in literature.²⁶ Recently, the nanocomposite CuO-CuFe₂O₄ has been synthesized in a single stage by one pot polyol method. The electrical, structural and optical properties of the synthesized CuO-CuFe₂O₄ were investigated as a function of different annealing temperatures ranges from 200–1000 °C.²⁷ Furthermore, a novel and recyclable magnetic catalyst Cu₂O/nano-CuFe₂O₄ has been reported for the coupling of carbonyl compounds–alkynes–amines in order to synthesize propargylamines under solvent-free condition.²⁸ These studies gave us a direction to synthesize Cu₂O–CuFe₂O₄ particles with both Cu(I) and Cu(II) species, resulting in the fast activation of H₂O₂ to get hydroxyl radicals

HO· for the elimination of recalcitrant organic pollutant such as phenol.

In this study, we have explored a facile and novel method to fabricate Cu₂O–CuFe₂O₄ microparticles using Fenton sludge as iron source, which was further used as a heterogeneous catalyst in Fenton process for the elimination of recalcitrant phenol. Thus, the aims of the present study were (1) to fabricate and characterize Cu₂O–CuFe₂O₄, (2) to assess the catalytic activity of fabricated Cu₂O–CuFe₂O₄ in Fenton oxidation, (3) to investigate the synergetic effect of Cu(I)/Cu(II) as well as Fe(III)/Fe(II) redox pairs in Fenton reaction, and (4) to propose possible catalytic mechanism involved in efficient Fenton reaction at the presence of Cu₂O–CuFe₂O₄.

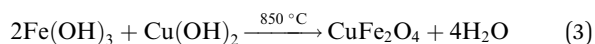
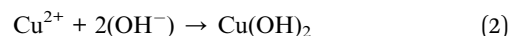
2. Materials and methods

2.1 Characteristics of the Fenton sludge used

The characteristics of iron-containing sludge obtained from neutralization process after Fenton oxidation could be described as follows. As a rich iron source, total iron content of Fenton sludge used for the synthesis of Fenton catalyst was as high as 8.65 ± 0.78 g L⁻¹. Chemical oxygen demand (COD) concentration of the Fenton sludge used was about 6700 ± 375 mg L⁻¹. The higher COD value exhibited the presence of abundant organics in Fenton sludge. Moreover, the Fenton sludge used in this study could be fluidized in nature, having total solid as well as water content of about 87.48% ± 0.97% and 12.52 ± 0.97%, respectively.

2.2 Synthesis of CuFe₂O₄ microparticles

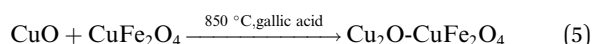
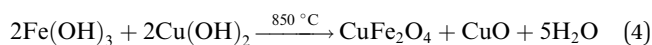
CuFe₂O₄ microparticles were prepared by co-precipitation technique, *i.e.*, CuSO₄·5H₂O was dissolved into ultrapure water and then the prepared CuSO₄ solution was mixed with Fenton sludge at Fe/Cu molar ratio of 2 : 1. Thereafter, sodium hydroxide solution (5 mol L⁻¹) was added into the mixture of Fenton sludge and CuSO₄ drop by drop under continuous stirring to raise the pH value to 10.0. The mixture was stirred continuously at temperature of 65 °C for 2 h. The obtained precipitate was then separated by centrifugation and washed with ultrapure water until the pH value of the filtrate reached 7.0. The resulting product was kept in an oven at temperature of 105 °C for 3 h to make it dry and then finally sintered at 850 °C for 3 h under nitrogen atmosphere. The formation of CuFe₂O₄ microparticles could be described by eqn (1)–(3):



2.3 Synthesis of Cu₂O–CuFe₂O₄ microparticles

Cu₂O–CuFe₂O₄ microparticles were prepared through modified hydrothermal technique.²⁹ In this case, CuSO₄·5H₂O solution and Fenton sludge were mixed together at Fe/Cu molar ratio of

1 : 1. Sodium hydroxide solution (5 mol L⁻¹) was added drop wise into the mixture of Fenton sludge and CuSO₄ under continuous stirring to raise the pH value to 10.0 to get colloidal suspension. After this, 0.97 g gallic acid was blended with the suspension. The obtained mixture was sonicated for 15 min and then was poured into a 200 mL Teflon-line stainless steel autoclave. The closed autoclave was then allowed to keep at 200 °C for almost 12 h and finally cooled normally to room temperature. During hydrothermal process the gallic acid attached with chemical substances as organic ligands. The obtained product was separated and washed several times with ultrapure water, then dried at 105 °C and finally sintered at 850 °C for 3 h under nitrogen atmosphere. The calcination temperature was chosen as 850 °C because higher temperature causes lower reactivity and lower temperature favors severe leaching from catalysts.³⁰ Moreover, for comparison purpose, the Cu₂O microparticles was synthesized in a similar way by using CuSO₄·5H₂O individually as a precursor material. The formation of Cu₂O–CuFe₂O₄ microparticles could be described by eqn (4) and (5):



2.4 Catalytic degradation experiment

Catalytic degradation of phenol was carried out in a series of 100 mL centrifuge tubes. 50 mL phenol solution at initial concentration of 250 mg L⁻¹ and initial pH of 4.0 was added into these centrifuge tubes. Fenton reaction was initiated by adding H₂O₂ and magnetic heterogeneous Fenton catalyst into phenol solution. The initial concentration of H₂O₂ and magnetic heterogeneous Fenton catalyst was set at 80 mmol L⁻¹ and 2 g L⁻¹, respectively. The Fenton reaction was carried out on a rotary shaker at 30 °C and 220 rpm. The heterogeneous Fenton catalyst was recovered from solution after the reaction by applying external magnetic field for expected reuse. The control experiments carried out with Fenton catalyst but without H₂O₂ or with H₂O₂ but without Fenton catalyst were performed in the same manner.

2.5 Characterization and analytical methods

Total iron content of Fenton sludge, copper and iron leaching were analyzed through Inductive Couple Plasma Optical Emission Spectrometer (ICP-OES) (Optima 7000DV, PerkinElmer, USA). A mixture of 2.5 mL HClO₄, 2.5 mL HNO₃ (69%) and 10 mL HF (40%) was used for wet digestion of Fenton sludge. The COD concentration of Fenton sludge was analyzed by the standard potassium dichromate method. SEM (JSM-6380, JEOL, Japan) and HRTEM (FEI Philips CM300 UT/FEG) were applied to characterize the surface morphology, size and shape of as prepared CuFe₂O₄ and Cu₂O–CuFe₂O₄ microparticles. BET (Micromeritics, ASAP 2020, USA) surface area was quantified by nitrogen adsorption data at 77 K. For the investigation of crystal structure of as-prepared materials, XRD (D8 Advance, Burker,

Germany) analysis was performed. X-Ray Photoelectron Spectroscopy (XPS, ESCALAB 250) technique was implemented to determine the synthesized materials elemental composition and different oxidation states of corresponding elements. The magnetic strength was tested on a vibrating sample magnetometer (VSM) (Lake Shore 7410, Lake Shoe Cryotronics, Inc. USA). Phenol identification and quantification was carried out by high performance liquid chromatography (HPLC) (Waters 2996, Waters Incorporation, USA). Identification of intermediates formed during phenol degradation was confirmed by GC-MS as well as HPLC.

3. Results and discussion

3.1 Characterization of the synthesized microparticles

In this study, the CuFe₂O₄ and Cu₂O–CuFe₂O₄ microparticles were synthesized by co-precipitation and modified hydrothermal method followed by sintering under nitrogen atmosphere. Fig. 1 showed the SEM and high resolution TEM images of CuFe₂O₄ and Cu₂O–CuFe₂O₄ microparticles. It was obvious that only one type of specific shape agglomerated particles could be observed in case of synthesized CuFe₂O₄ microparticles (Fig. 1(a)). However, for Cu₂O–CuFe₂O₄ microparticles, two different types of agglomerated particles could be observed and the new types of agglomerated particles were pointed out with red arrows in SEM image (Fig. 1(b)). Similar evidence was revealed by high resolution TEM images (Fig. 1(c) and (d)). Two different particles were existed in case of Cu₂O–CuFe₂O₄ microparticles as compared to CuFe₂O₄ microparticles, the results were in agreement with SEM images. Through comparison between both synthesized particles and literature review, it was speculated that the microparticles with the shape like chrysanthemum might be Cu₂O, which should be further clarified by XRD analysis. The Cu/Cu₂O/CuO@C catalyst particles recently synthesized by Zhao *et al.*, which had excellent catalytic performance, was also similar to chrysanthemum as in our case.³¹ BET surface area analysis was also carried out for the synthesized heterogeneous catalysts, as indicated in Table 1. The BET surface area (1.08 m² g⁻¹) for CuFe₂O₄ particles was smaller than that of Cu₂O–CuFe₂O₄ particles (1.65 m² g⁻¹), which might be directed towards the generation of additional chrysanthemum shaped Cu₂O particles along with CuFe₂O₄ particles at the presence of gallic acid. The presence of puffy ball-like structure particles might result in higher BET surface area of Cu₂O–CuFe₂O₄ particles. For synthesized Cu₂O micro particles the BET surface area was 1.50 m² g⁻¹ which was higher than that of CuFe₂O₄ (1.08 m² g⁻¹). It could be referred to puffy ball like shape of Cu₂O particles.

XRD analysis was carried out to examine the crystal phase and structure of synthesized products (Fig. 2). The diffraction peaks appeared at 2θ of 18.5° (111), 30.2° (220), 35.6° (311), 37.2° (222), 43.0° (400), 57.1° (511), 62.8° (440) and 74.5° (533) could be assigned to pure cuprospinel CuFe₂O₄ (JCPDS#25-0283). In comparison with pure cuprospinel CuFe₂O₄, newly originated diffraction peaks positioning at 2θ of 36.7° (111), 42.5° (200), 61.6° (220) and 73.7° (311) could be attributed to rhombic dodecahedral crystal of Cu₂O (JCPDS#05-0667) in

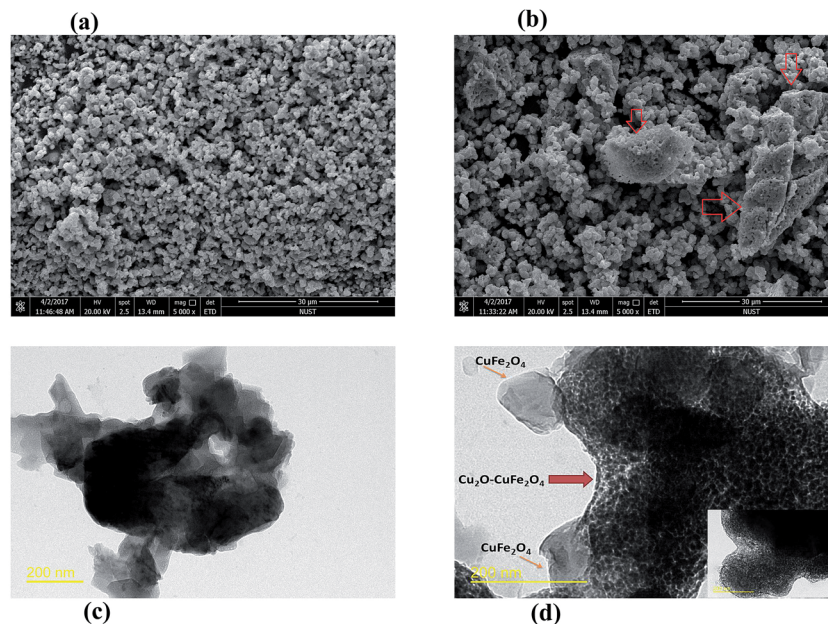


Fig. 1 SEM (a, b) and high resolution TEM (c, d) images of CuFe_2O_4 and $\text{Cu}_2\text{O}-\text{CuFe}_2\text{O}_4$.

cubic phase, which confirmed the existence of Cu_2O in as-synthesized $\text{Cu}_2\text{O}-\text{CuFe}_2\text{O}_4$.

XPS technique was applied for thorough study of chemical composition and different oxidation states of constituent elements of synthesized materials. From XPS wide spectrum in Fig. 3(a), it was clear that both microparticles were comprised of same parent constituents, such as Fe, Cu and O elements. Someone could differentiate between materials having the same parent constituents on the behalf of different oxidation states of existed constituent elements. For example, existence of Cu^{2+} in CuFe_2O_4 and the presence of Cu^+ in $\text{Cu}_2\text{O}-\text{CuFe}_2\text{O}_4$ materials could be confirmed on the behalf of different binding energy of Cu^{2+} and Cu^+ , respectively. As shown in Fig. 3(b), the detail XPS spectra of Cu 2p reveals that strong Cu^{2+} satellites could be observed at binding energy of 942.5 eV and 962.5 eV along with peak at 934.3 eV, which confirmed the presence of Cu^{2+} in CuFe_2O_4 .^{32,33} In addition, on the basis of the relatively weak peak at 932.1 eV,³⁴ there were Cu^+ species on the surface of CuFe_2O_4 , which might come from the reduction of Cu^{2+} during calcination process due to the abundant organics in Fenton sludge. In contrast, for $\text{Cu}_2\text{O}-\text{CuFe}_2\text{O}_4$, there was a relatively strong peak at 932.1 eV in Fig. 3(c), which could be referred to Cu_2O . Similar result was found for Cu/ Cu_2O /CuO@C catalyst particles.³¹ In addition, peak at 934.3 eV and weak satellite peaks at 942.5 eV and 962.5 eV confirm the

formation of Cu^{2+} along with CuFe_2O_4 particles for as-prepared $\text{Cu}_2\text{O}-\text{CuFe}_2\text{O}_4$ microparticles. Moreover, for wide scan of Fe 2p spectra, the peaks raised at 711.4 eV along with shakeup satellite pointed at 719.9 eV corresponded to the existence of Fe^{3+} cations. However, XPS spectrum for Fe 2p and O 1s for both CuFe_2O_4 and $\text{Cu}_2\text{O}-\text{CuFe}_2\text{O}_4$ were similar, as shown in Fig. 3(a) and (d).

The magnetic property of the as-prepared $\text{Cu}_2\text{O}-\text{CuFe}_2\text{O}_4$ and CuFe_2O_4 was determined by applied field of $\pm 10\,000$ Oe. As shown in Fig. (4), the saturation magnetization and coercivity values for as-prepared $\text{Cu}_2\text{O}-\text{CuFe}_2\text{O}_4$ and CuFe_2O_4 were 71 emu g^{-1} and 73 Oe, 61 emu g^{-1} and 50 Oe, respectively. The magnetic hysteresis loop exhibited better ferromagnetic behavior of $\text{Cu}_2\text{O}-\text{CuFe}_2\text{O}_4$ as compared to CuFe_2O_4 . The material having magnetic features could be easily separated by external applied magnetic field for possible reuse. CuFe_2O_4 nanoparticles synthesized by Phuruangrat *et al.* through microwave-hydrothermal method showed a maximum saturation magnetization of about 56 emu g^{-1} .³⁵ Higher saturation magnetization values of $\text{Cu}_2\text{O}-\text{CuFe}_2\text{O}_4$ observed in this study could be attributed to the presence of additional Cu_2O in CuFe_2O_4 particles. Previous study about the magnetic property of Cu_2O has confirmed that Cu_2O could act as a diamagnetic to ferromagnetic depending upon the role of native defects in bulk Cu_2O .³⁶

Table 1 Catalyst or catalysts physicochemical properties, their catalytic performance and metals ions leaching

Catalyst	BET S. area ($\text{m}^2\text{ g}^{-1}$)	Average particle size (μm)	TOC removal (%)	Phenol removal (%)	Iron leaching (mg L^{-1})	Copper leaching (mg L^{-1})
CuFe_2O_4	1.08	2–3	47.6 ± 1.0	57.8 ± 3.6	1.16	30.18
$\text{Cu}_2\text{O}-\text{CuFe}_2\text{O}_4$	1.65	0.5–2	85.6 ± 0.7	97.2 ± 0.4	1.53	28.60
Cu_2O	1.50	2–3.5	36.5 ± 1.5	61.9 ± 2.3	—	—

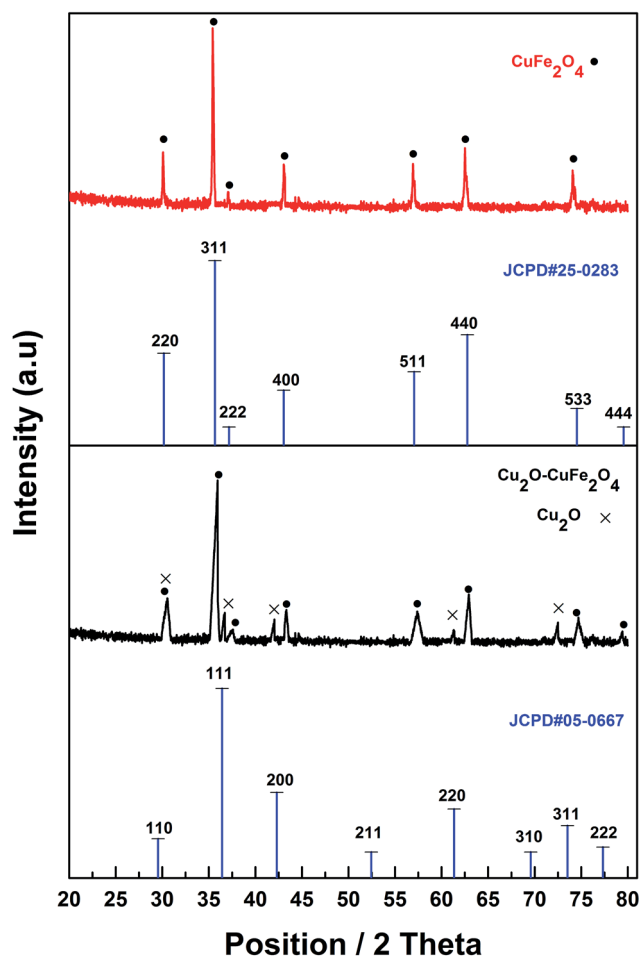


Fig. 2 XRD of CuFe_2O_4 and $\text{Cu}_2\text{O}-\text{CuFe}_2\text{O}_4$.

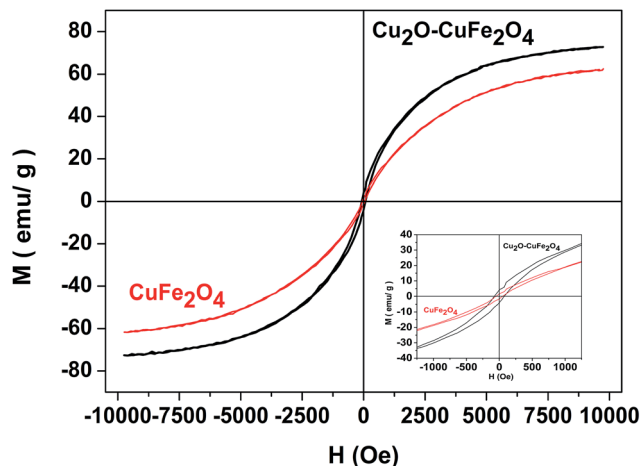


Fig. 4 Hysteresis curve for $\text{Cu}_2\text{O}-\text{CuFe}_2\text{O}_4$ and CuFe_2O_4 .

3.2 Heterogeneous Fenton performance of $\text{Cu}_2\text{O}-\text{CuFe}_2\text{O}_4$

Heterogeneous Fenton performance of the catalyst prepared was mainly dependent on the potential to generate hydroxyl radical (OH^\bullet) through H_2O_2 decomposition. As shown in Fig. 5(a), in the system with H_2O_2 alone but without CuFe_2O_4 or $\text{Cu}_2\text{O}-\text{CuFe}_2\text{O}_4$, phenol removal efficiency within 60 min was as low as $6.4 \pm 0.6\%$, indicating the poor oxidation ability of H_2O_2 alone toward phenol. In the control experiments without H_2O_2 but with CuFe_2O_4 and $\text{Cu}_2\text{O}-\text{CuFe}_2\text{O}_4$, phenol removal efficiencies were $11.4 \pm 1.7\%$ and $13.8 \pm 1.0\%$, respectively, which could be attributed to the adsorption of phenol by as-prepared CuFe_2O_4 and $\text{Cu}_2\text{O}-\text{CuFe}_2\text{O}_4$. When CuFe_2O_4 and Cu_2O were utilized in the presence of H_2O_2 , phenol removal efficiency within 60 min was significantly increased to $57.8 \pm 3.6\%$ and

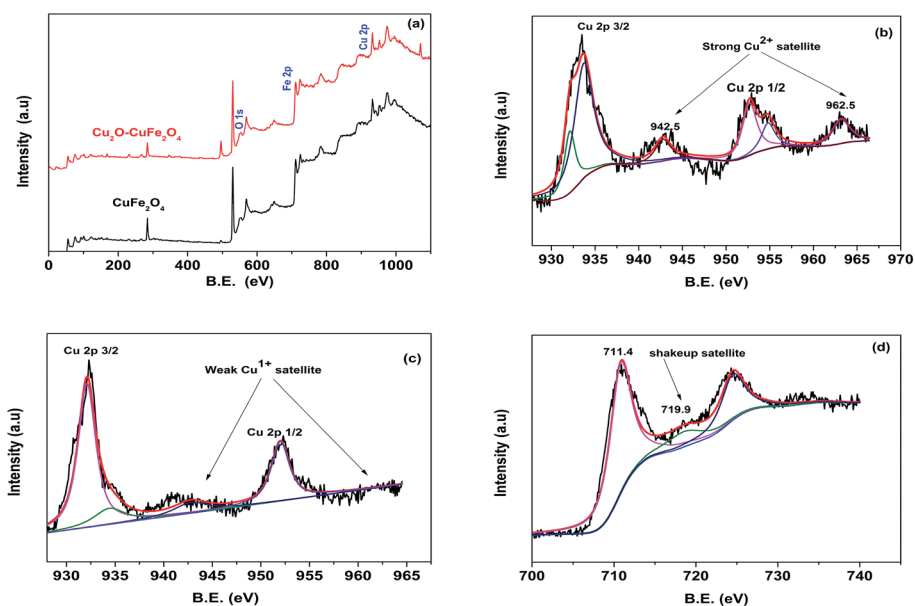


Fig. 3 XPS spectra for CuFe_2O_4 and $\text{Cu}_2\text{O}-\text{CuFe}_2\text{O}_4$ (a), strong Cu^{2+} satellite for CuFe_2O_4 (b), weak Cu^{1+} satellite for $\text{Cu}_2\text{O}-\text{CuFe}_2\text{O}_4$ (c), similar Fe 2p region for both CuFe_2O_4 and $\text{Cu}_2\text{O}-\text{CuFe}_2\text{O}_4$ (d).

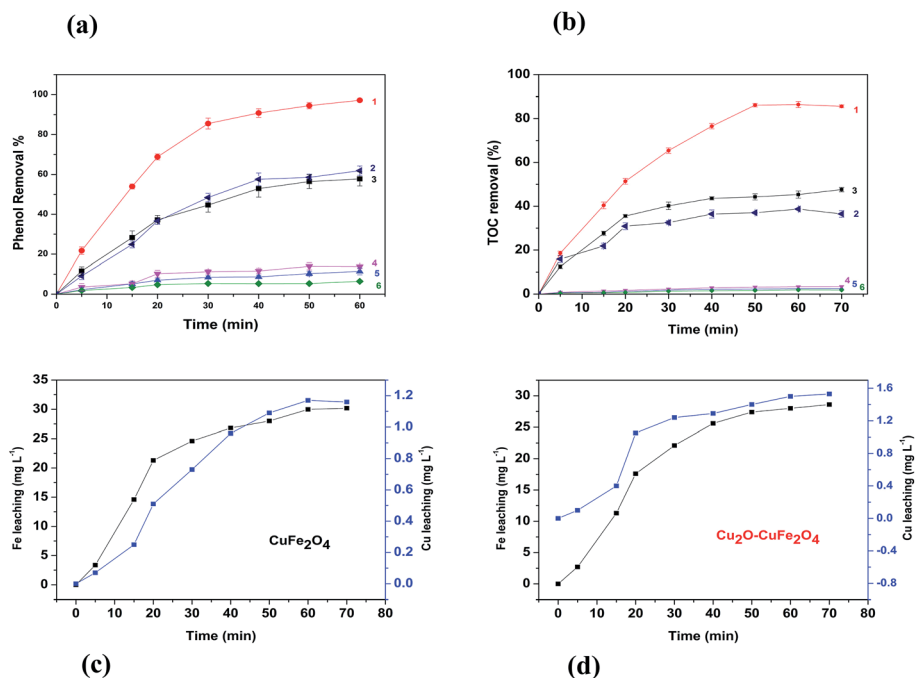


Fig. 5 Catalysts performance for phenol removal (a), TOC removal (b), iron and copper leaching for CuFe₂O₄ (c) and Cu₂O-CuFe₂O₄ (d). (1): Cu₂O-CuFe₂O₄ + H₂O₂; (2): Cu₂O + H₂O₂ (3): CuFe₂O₄ + H₂O₂; (4): Cu₂O-CuFe₂O₄ alone; (5) CuFe₂O₄ alone; (6) H₂O₂ alone.

61.9 ± 2.3%, respectively, indicating the positive role of CuFe₂O₄ and Cu₂O in phenol oxidation by H₂O₂. In case of Cu₂O, slightly higher phenol removal efficiency as compared to CuFe₂O₄ could be attributed to more active site availability due to higher surface area and relatively more generation of HO· radical than HO₂· as a result of monovalent copper Cu(I). Moreover, When Cu₂O-CuFe₂O₄ was used as Fenton catalyst, phenol removal efficiency increased sharply within 30 min to 85.5 ± 2.8% and further increased to 97.2 ± 0.4% within 60 min. When Cu₂O-CuFe₂O₄ was used as the catalyst for phenol oxidation by H₂O₂, a remarkable increase in terms of phenol removal indicated better catalysis performance of Cu₂O-CuFe₂O₄ than CuFe₂O₄ and Cu₂O.

Moreover, TOC removal observed in heterogeneous Fenton system followed the similar trend. As indicated in Fig. 5(b), in the Fenton system with H₂O₂ alone, with CuFe₂O₄ alone and with Cu₂O-CuFe₂O₄ alone, TOC removal efficiencies within 60 min were as low as 1.8 ± 0.1%, 2.5 ± 0.1%, 3.4 ± 0.1%, respectively. However, in Fenton system catalyzed by Cu₂O, CuFe₂O₄, and Cu₂O-CuFe₂O₄, TOC removal efficiencies within 60 min were as high as 36.5 ± 1.5%, 47.6 ± 1.0% and 85.6 ± 0.7%, respectively. Nevertheless, no remarkable increase of TOC removal efficiencies could be observed when reaction time prolonged to 70 min. TOC removal performance confirmed the amazing catalytic activity of CuFe₂O₄ and Cu₂O-CuFe₂O₄ towards H₂O₂ oxidation, especially for Cu₂O-CuFe₂O₄.

Fenton and Cu²⁺ coupled system has been studied for the enhanced mineralization of phenol, with phenol removal efficiency as high as 94% was achieved in Fenton-Cu²⁺ system at initial phenol concentration of 100 mg L⁻¹.^{24,37} In addition, Stoia *et al.* prepared MnFe₂O₄ nanoparticles, which was used for

the oxidative degradation of phenol at initial concentration of about 50 mg L⁻¹.³⁸ Phenol removal efficiency of 90% could be achieved at pH of 3.0–3.5 under the catalyst dosage of 3 g L⁻¹. In this study, phenol removal efficiency as high as 97.2 ± 0.4% could be achieved within 60 min at the presence of Cu₂O-CuFe₂O₄, even at initial phenol concentration as high as 250 mg L⁻¹. The relatively higher catalytic role of Cu₂O-CuFe₂O₄ obtained in this study could be attributed to the coexistence of both monovalent copper [Cu(I)] and divalent copper [Cu(II)] in the structure of Cu₂O-CuFe₂O₄.

3.3 Sound stability and reusability of Cu₂O-CuFe₂O₄

Leaching study for the as-prepared CuFe₂O₄ and Cu₂O-CuFe₂O₄ was carried out to investigate their stability and reusability, as shown in Fig. 5(c) and (d). The concentration of leached iron at pH 4.0 for CuFe₂O₄ and Cu₂O-CuFe₂O₄ was 30.18 mg L⁻¹ and 28.60 mg L⁻¹, accounted for 3.22% and 4.77% of the total iron contents at applied catalyst dosage of 2.0 g L⁻¹. Moreover, for CuFe₂O₄ and Cu₂O-CuFe₂O₄, the observed copper leaching was 1.16 mg L⁻¹ and 1.53 mg L⁻¹, accounted for 0.22% and 0.15% of total copper contents at applied catalyst dosage of 2.0 g L⁻¹. Although the iron leaching for Cu₂O-CuFe₂O₄ was a little higher than that of CuFe₂O₄, the observed copper leaching for Cu₂O-CuFe₂O₄ was lower than that of CuFe₂O₄. Therefore, Cu₂O-CuFe₂O₄ microparticles show good stability as compared to CuFe₂O₄ considering the low leaching of copper. In addition, these values for iron and copper leaching observed in this study were relatively lower than those reported in the literature. For example, the iron leaching accounted for 5.08% of the total iron contents at applied catalyst dosage of 0.24 g L⁻¹ has been

reported in literature, where ferrite particles were applied as heterogeneous Fenton catalyst for the degradation of Rhodamine B.³⁹ Fontecha-Cámara *et al.* applied mixed iron oxide as Fenton catalyst in order to remove gallic acid from aqueous solutions.⁴⁰ The observed copper leaching for copper ferrite was 2.85 mg L^{-1} at pH 4.3, which accounted for 21.50% of the total copper contents at applied catalyst dosage of 0.05 g L^{-1} . As for the reusability, $\text{Cu}_2\text{O-CuFe}_2\text{O}_4$ exhibited a slight decrease in phenol degradation efficiency (from $97.2 \pm 0.4\%$ to $85.7 \pm 0.5\%$) within five consecutive runs, as shown in Fig. 6(a). However, in case of CuFe_2O_4 , a sharp decrease of phenol removal efficiency (from $57.77 \pm 3.55\%$ to $32.32 \pm 1.55\%$) was observed even after three cycles, as indicated in Fig. 6(b). The decrease in phenol degradation efficiency was due to vanishing of available active site on CuFe_2O_4 surface after reuse, which could be overcome through the incorporation of Cu_2O in CuFe_2O_4 structure.

3.4 The possible mechanism involved in Fenton reaction by $\text{Cu}_2\text{O-CuFe}_2\text{O}_4$

Based on the above results, the possible mechanism involved in Fenton reaction by $\text{Cu}_2\text{O-CuFe}_2\text{O}_4$ could be described in Fig. 7. In our case, the available Fe(III) on both CuFe_2O_4 and $\text{Cu}_2\text{O-CuFe}_2\text{O}_4$ surface was firstly reduced into Fe(II) due to its reaction with adsorbed H_2O_2 on the surface of both microparticles. The desired HO^\bullet radical was produced when the generated Fe(II) further reacted with H_2O_2 in a similar way, which was known as

Haber-Weiss process.⁴¹ Literature study reveals that conversion of Fe(III) to Fe(II) was very slow when compared with the conversion of Fe(II) to Fe(III) .⁴² The presence of transition metal copper in the skeleton of spinel catalyst may enhance phenol degradation due to availability of Cu(II)/Cu(I) redox pairs, which causes acceleration of the redox cycle of Fe(III)/Fe(II) ions at room temperature. Zhang *et al.* prepared CuFe_2O_4 microparticles for the degradation of bisphenol A, confirming the effectiveness of Cu(I) species as compare to Cu(II) species for the activation of H_2O_2 to generate HO^\bullet radicals.²⁶ As indicated in literature study, the reaction rate constant (k) between monovalent copper [Cu(I)] and H_2O_2 was as high as $1.0 \times 10^4 \text{ M}^{-1} \text{ s}^{-1}$, as compared to that between divalent copper [Cu(II)] and H_2O_2 , which was as low as $4.6 \times 10^2 \text{ M}^{-1} \text{ s}^{-1}$.⁴³ In our study, the generation of reactive HO^\bullet radical may start by ligand displacement between the hydrous surface of $\text{Fe}^{\text{III}}\text{-OH/Cu}^{\text{II}}\text{-OH}$ and H_2O_2 , with the generation of $\text{Fe}^{\text{III}}\text{-H}_2\text{O}_2$ and $\text{Cu}^{\text{II}}\text{-H}_2\text{O}_2$. Then initially generated $\text{Fe}^{\text{III}}\text{-H}_2\text{O}_2$ and $\text{Cu}^{\text{II}}\text{-H}_2\text{O}_2$ species can produce HO_2^\bullet and regenerate Fe^{II} and Cu^{I} by intramolecular electron transfer, which subsequently produced HO^\bullet and degraded phenol. The hydroxyl radicals HO^\bullet were considered as major oxidizing species for phenol mineralization and HO_2^\bullet radicals as minor oxidizing species. The generation route for major and minor oxidizing species, and proposed mechanism for phenol degradation could be described by eqn (6)–(15):

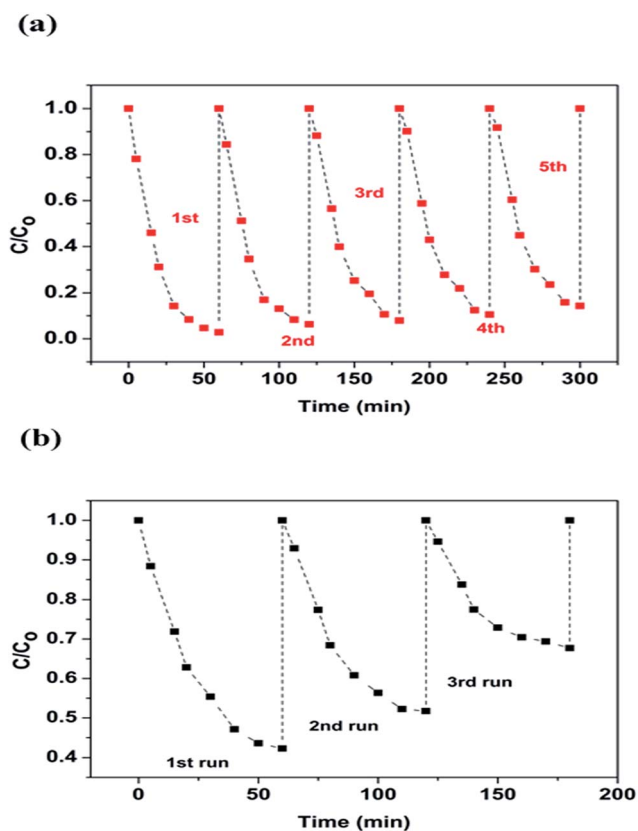
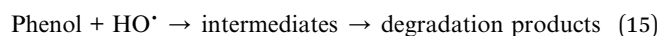
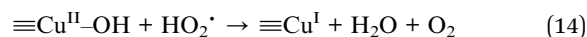
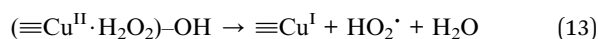
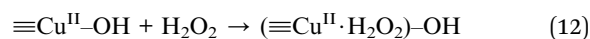
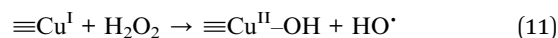
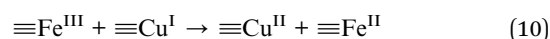
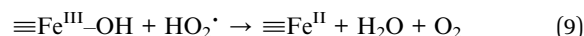
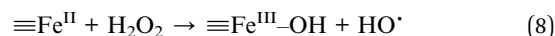
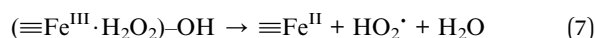
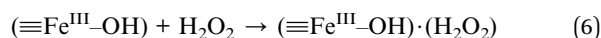


Fig. 6 Reusability study for $\text{Cu}_2\text{O-CuFe}_2\text{O}_4$ (a) and CuFe_2O_4 (b).

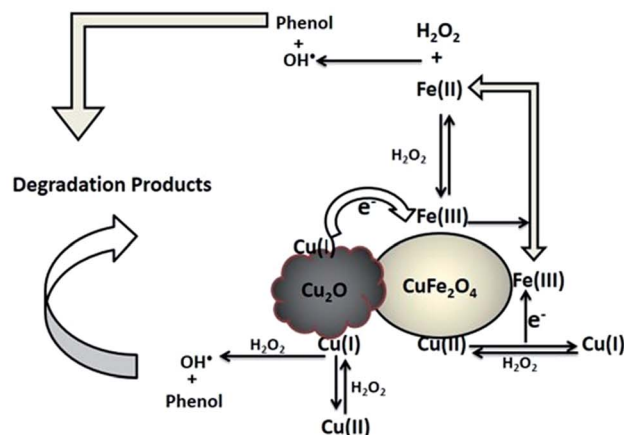
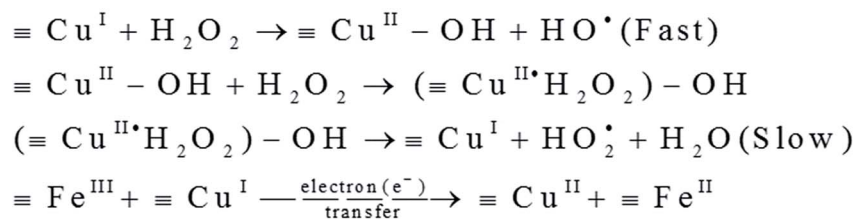


Fig. 7 Possible mechanisms for phenol degradation in Fenton system based on $\text{Cu}_2\text{O}-\text{CuFe}_2\text{O}_4$.

production of highly reactive radical HO^\bullet as compared to HO_2^\bullet species. For the mineralization of carbamazepine, Ding *et al.* prepared recyclable CuFeO_2 microparticles for heterogeneous activation of peroxymonosulfate (PMS) in order to generate sulfate radicals ($\text{SO}_4^{\bullet-}$). It was concluded that enhanced activation of PMS by micro- CuFeO_2 referred to synergetic effect of surface $\text{Cu}(\text{i})$ and $\text{Fe}(\text{iii})$.⁴⁴ The higher Fenton activity by $\text{Cu}_2\text{O}-\text{CuFe}_2\text{O}_4$ might also be attributed to faster reaction rate between $\text{Cu}(\text{i})$ and H_2O_2 due to presence of additional Cu_2O particles, which results in faster reduction of H_2O_2 in order to generate highly reactive radical species HO^\bullet . The faster reduction of H_2O_2 due to presence of Cu_2O additional particles in case of $\text{Cu}_2\text{O}-\text{CuFe}_2\text{O}_4$ microparticles causes the relatively efficient consumption of H_2O_2 due to more available and highly reactive $\text{Cu}(\text{i})$ species.

4. Conclusion

The present work focus on the synthesis of a heterogeneous Fenton catalyst, namely $\text{Cu}_2\text{O}-\text{CuFe}_2\text{O}_4$, for the reuse of iron incorporated in Fenton sludge. In comparison to CuFe_2O_4 , much higher phenol catalytic degradation was found for $\text{Cu}_2\text{O}-\text{CuFe}_2\text{O}_4$, indicating the key role of Cu_2O in Fenton reaction. The rapid electron transfer built up galvanic cell between $\text{Cu}(\text{i})$ and $\text{Fe}(\text{iii})$, which favored the formation of relatively excess $\text{Fe}(\text{ii})$ species. The highly reactive $\text{Fe}(\text{ii})$ species interaction with adsorbed H_2O_2 gave abundant HO^\bullet radicals for phenol degradation. The higher Fenton catalytic activity of $\text{Cu}_2\text{O}-\text{CuFe}_2\text{O}_4$ could be attributed to the synergetic effect between $\text{Cu}(\text{i})/\text{Cu}(\text{ii})$ and $\text{Fe}(\text{ii})/\text{Fe}(\text{iii})$ redox pairs. The as prepared $\text{Cu}_2\text{O}-\text{CuFe}_2\text{O}_4$ was stable, recoverable and reusable, offering a promising potential as a heterogeneous Fenton catalyst.

Conflicts of interest

There are no conflicts of interest to declare.

Acknowledgements

This research is financed by Natural Science Foundation of Jiangsu Province for Distinguished Young Scholars (BK20170038), National Natural Science Foundation of China (51708293) and Natural Science Foundation of Jiangsu Province (BK20170842).

References

- 1 J. Xu, Y. Long, D. Shen, H. Feng and T. Chen, *J. Hazard. Mater.*, 2017, **323**, 674–680.
- 2 D. Gümüş and F. Akbal, *Process Saf. Environ. Prot.*, 2016, **103**, 252–258.
- 3 J. He, X. Yang, B. Men and D. Wang, *J. Environ. Sci.*, 2016, **39**, 97–109.
- 4 W. M. Wang, J. Song and X. Han, *J. Hazard. Mater.*, 2013, **262**, 412–419.
- 5 E. Mousset, L. Frunzo, G. Esposito, E. D. van Hullebusch, N. Oturan and M. A. Oturan, *Appl. Catal., B*, 2016, **180**, 189–198.
- 6 X. J. Ma and H. L. Xia, *J. Hazard. Mater.*, 2009, **162**, 386–390.
- 7 Y. Li, Y. Zhang, J. Li and X. Zheng, *Environ. Pollut.*, 2011, **159**, 3744–3749.
- 8 J. Feng, X. Hu, P. L. Yue and S. Qiao, *Sep. Purif. Technol.*, 2009, **67**, 213–217.
- 9 E. Garrido-Ramírez, B. Theng and M. Mora, *Appl. Clay Sci.*, 2010, **47**, 182–192.

- 10 M. Tekbaş, H. C. Yatmaz and N. Bektaş, *Microporous Mesoporous Mater.*, 2008, **115**, 594–602.
- 11 M. Aleksić, H. Kušić, N. Koprivanac, D. Leszczynska and A. L. Božić, *Desalination*, 2010, **257**, 22–29.
- 12 W. Wang, M. Zhou, Q. Mao, J. Yue and X. Wang, *Catal. Commun.*, 2010, **11**, 937–941.
- 13 H.-C. Yoo, S.-H. Cho and S.-O. Ko, *J. Environ. Sci. Health, Part A: Environ. Sci. Eng.*, 2001, **36**, 39–48.
- 14 S. Guo, N. Yuan, G. Zhang and J. C. Yu, *Microporous Mesoporous Mater.*, 2017, **238**, 62–68.
- 15 H. Zhang, G. Xue, H. Chen and X. Li, *Chemosphere*, 2018, **191**, 64–71.
- 16 R. C. Costa, M. d. F. F. Lelis, L. C. Oliveira, J. D. Fabris, J. D. Ardisson, R. R. Rios, C. N. Silva and R. M. Lago, *Catal. Commun.*, 2003, **4**, 525–529.
- 17 T. Giannakopoulou, L. Kompotiatis, A. Kontogeorgakos and G. Kordas, *J. Magn. Magn. Mater.*, 2002, **246**, 360–365.
- 18 M. Rashad and O. Fouad, *Mater. Chem. Phys.*, 2005, **94**, 365–370.
- 19 E. Hasmonay, J. Depeyrot, M. Sousa, F. Tourinho, J.-C. Bacri, R. Perzynski, Y. L. Raikher and I. Rosenman, *J. Appl. Phys.*, 2000, **88**, 6628–6635.
- 20 N. Rezlescu, N. Iftimie, E. Rezlescu, C. Doroftei and P. Popa, *Sens. Actuators, B*, 2006, **114**, 427–432.
- 21 F. Zhang, C. Wei, Y. Hu and H. Wu, *Sep. Purif. Technol.*, 2015, **156**, 625–635.
- 22 Y. Ding, L. Zhu, S. Wang and H. Tang, *Appl. Catal., B*, 2013, **129**, 153–162.
- 23 Y. Wang, H. Zhao and G. Zhao, *Appl. Catal., B*, 2015, **164**, 396–406.
- 24 H. Zhang, J. Liu, C. Ou, Faheem, J. Shen, H. Yu, Z. Jiao, W. Han, X. Sun, J. Li and L. Wang, *J. Environ. Sci.*, 2017, **53**, 1–8.
- 25 P. Roonasi and A. Y. Nezhad, *Mater. Chem. Phys.*, 2016, **172**, 143–149.
- 26 X. Zhang, Y. Ding, H. Tang, X. Han, L. Zhu and N. Wang, *Chem. Eng. J.*, 2014, **236**, 251–262.
- 27 K. Ramachandran, S. Chidambaram, B. Baskaran, A. Muthukumarasamy and G. M. Kumar, *Mater. Lett.*, 2016, **175**, 106–109.
- 28 F. Nemat, A. Elhampour, H. Farrokhi and M. B. Natanzi, *Catal. Commun.*, 2015, **66**, 15–20.
- 29 X. Qiu, M. Liu, K. Sunada, M. Miyauchi and K. Hashimoto, *Chem. Commun.*, 2012, **48**, 7365–7367.
- 30 J. Du, J. Bao, X. Fu, C. Lu and S. H. Kim, *Sep. Purif. Technol.*, 2016, **11**, 145–152.
- 31 X. Zhao, Y. Tan, F. Wu, H. Niu, Z. Tang, Y. Cai and J. P. Giesy, *Sci. Total Environ.*, 2016, **571**, 380–387.
- 32 L. Huang, F. Peng and F. S. Ohuchi, *Surf. Sci.*, 2009, **603**, 2825–2834.
- 33 Z. Ai, L. Zhang, S. Lee and W. Ho, *J. Phys. Chem. C*, 2009, **113**, 20896–20902.
- 34 C. D. Wagner and G. Muilenberg, *Handbook of X-ray photoelectron spectroscopy*, Perkin-Elmer, 1979.
- 35 A. Phuruangrat, B. Kuntalue, S. Thongtem and T. Thongtem, *Mater. Lett.*, 2016, **167**, 65–68.
- 36 X. Yu, X. Zhang, S. Wang and G. Feng, *Curr. Appl. Phys.*, 2015, **15**, 1303–1311.
- 37 J. Maekawa, K. Mae and H. Nakagawa, *J. Environ. Chem. Eng.*, 2014, **2**, 1275–1280.
- 38 M. Stoia, C. Muntean and B. Militaru, *J. Environ. Sci.*, 2016, **53**, 269–277.
- 39 T. R. Giraldi, C. C. Arruda, G. M. da Costa, E. Longo and C. Ribeiro, *J. Sol-Gel Sci. Technol.*, 2009, **52**, 299–303.
- 40 M. A. Fontecha-Cámara, C. Moreno-Castilla, M. V. López-Ramón and M. A. Álvarez, *Appl. Catal., B*, 2016, **196**, 207–215.
- 41 S.-S. Lin and M. D. Gurol, *Environ. Sci. Technol.*, 1998, **32**, 1417–1423.
- 42 K. Li, Y. Zhao, M. J. Janik, C. Song and X. Guo, *Appl. Surf. Sci.*, 2017, **396**, 1383–1392.
- 43 A. D. Bokare and W. Choi, *J. Hazard. Mater.*, 2014, **275**, 121–135.
- 44 Y. Ding, H. Tang, S. Zhang, S. Wang and H. Tang, *J. Hazard. Mater.*, 2016, **317**, 686–694.